Nanoparticle Superlattice Engineering with DNA

Robert J. Macfarlane,[1,2] Byeongdu Lee,[3] Matthew R. Jones,[2,4] Nadine Harris,[1,2] George C. Schatz,[1,2] Chad A. Mirkin[1,2,3]*

A current limitation in nanoparticle superlattice engineering is that the identities of the particles being assembled often determine the structures that can be synthesized. Therefore, specific crystallographic symmetries or lattice parameters can only be achieved using specific nanoparticles as building blocks (and vice versa). We present six design rules that can be used to deliberately prepare nine distinct colloidal crystal structures, with control over lattice parameters on the 25- to 150-nanometer length scale. These design rules outline a strategy to independently adjust each of the relevant crystallographic parameters, including particle size (5 to 60 nanometers), periodicity, and interparticle distance. As such, this work represents an advance in synthesizing tailorable macroscale architectures comprising nanoscale materials in a predictable fashion.

The crystallographic lattice adopted by a given set of atomic and molecular components is often difficult to predict and control and is dependent on a large number of factors. For ionic solids, Pauling developed rules that explain the relative stabilities of different lattices of simple salts, but these rules do not allow for structure control (*1*). This is because parameters such as size and charge for atoms (and small molecules) are not tunable; changing an atom's size or charge inherently changes the electronic properties that affect relative lattice stability. In principle, nanoparticle-based superlattice materials should allow for more control over the types of crystal lattice that they adopt, given that one can tune multiple variables (such as nanoparticle size or the presence of different organic molecule layers on the nanoparticle surface) to control superlattice stability (*2*–*14*). Although advances have been made using a variety of electrostatic forces (*7*–*9*), covalent and noncovalent molecular interactions (*6*, *11*), and biologically driven assembly strategies (*2*–*5*, *12*), predictable architectural control remains an elusive goal, regardless of the type of particle interconnect strategy chosen. In 1996, the use of oligonucleotides as particle-directing motifs to synthesize amorphous polymeric materials from polyvalent particles modified with nucleic acids was demonstrated (*2*). Subsequent work showed that crystallization and lattice control were possible for face-centered cubic (fcc) and body-centered cubic (bcc) crystal structures simply by taking advantage of the programmable nature of DNA (both in base sequence and in overall oligonucleotide length) (*3*–*5*, *15*–*18*).

Herein, we describe a set of rules for using programmable oligonucleotide interactions, elements of both thermodynamic and kinetic control, and an understanding of the dominant forces that are responsible for particle assembly to design and deliberately make a wide variety of crystal types. Like the rules for atomic lattices developed by Pauling, these are guidelines for determining relative nanoparticle superlattice stability, rather than rigorous mathematical descriptions. However, unlike Pauling's rules, the set of rules below can be used not only to predict crystal stability but also to deliberately and independently control the nanoparticle sizes, interparticle spacings, and crystallographic symmetries of a superlattice (Fig. 1A). This methodology represents a major advance toward nanoparticle superlattice engineering, as it effectively separates the identity of a particle core (and thereby its physical properties) from the variables that control its assembly.

We used polyvalent conjugates of DNA and gold nanoparticles (DNA-NPs) as the basic building blocks for assembling superlattices, for which programmable recognition and hybridization interactions between DNA strands drive the assembly process (Fig. 1B). The key hypothesis in this work is that the maximization of DNA hybridization events between adjacent particles is a more important factor in determining lattice stability than all other forces in the system. Synthetically controllable variations in nucleotide sequence allowed us to change the overall hydrodynamic size and coordination environment (and thus the hybridization behavior) of the particles, without the need to alter the structure of the inorganic nanoparticle core (*2*–*5*, *15*–*18*). We used synchrotron-based small-angle x-ray scattering (SAXS) to characterize all lattices reported herein, because it allows for in situ analysis of highly solvated materials. We also have developed a complementary method to embed these superlattices in a resin, which enables their characterization by transmission electron microscopy (TEM) (*17*). However, we note that the embedding process results in a slight deformation and disordering of the lattices, and that it significantly reduces the crystal lattice parameters as determined with in situ SAXS measurements.

In a typical experiment, we assembled DNA-NP superlattices using oligonucleotide linker strands that, upon binding to a DNA-NP, present a short, single-stranded DNA "sticky end" at a controllable distance from the nanoparticle surface (*19*) (fig. S1 and table S1). This distance dictates the interparticle spacing in a programmable manner (*16*). Because of the polyvalent nature of the DNA-NPs, each NP hybridizes to multiple linker strands and subsequently forms tens to hundreds of sticky end duplexes to adjacent NPs, enabling the construction of lattices that are indefinitely stable under ambient conditions. However, because individual sticky end connections are weak (a single sticky end duplex is not stable on its own at room temperature) and therefore transient, upon thermal annealing, DNA-NPs can shift positions within the material to ultimately form ordered lattices (*15*). Although all of the structures we describe are made with gold NPs, the assembly process should also be applicable to any other NP that can be densely functionalized with oligonucleotides.

We determined structural characteristics for a total of 41 crystals that adopted one of nine crystal lattices. In addition to fcc and bcc structures, we also prepared the following lattices (*19*) (figs. S2 to S21 and S29 to S31): hexagonal close-packed (hcp); AB, isostructural with cesium chloride (CsCl); AB_2, isostructural with aluminum diboride; AB_3, isostructural with Cr_3Si; AB_6, isostructural with the alkali-fullerene complex Cs_6C_{60}; AB, isostructural with sodium chloride (NaCl); and simple cubic (sc). For each structure, we could tune lattice parameters by means of independent modifications to both oligonucleotide interconnect length and nanoparticle size. Rather than discuss each group of structures in turn (*19*), we describe a set of rules that constitute a design strategy for synthesizing a particular choice of one of the nine distinct crystallographic symmetries.

Rule 1: *When all DNA-NPs in a system possess equal hydrodynamic radii, each NP in the thermodynamic product will maximize the number of nearest neighbors to which it can form DNA connections*. This occurs because maximizing the number of nearest neighbors in these systems in turn maximizes the number of potential DNA connections between nanoparticles, which we have hypothesized to be the driving force in forming ordered crystals. When using linkers with self-complementary sticky ends, where all particles can bind to all other particles in solution, the observed thermodynamic product is always an fcc lattice (Fig. 1C), a conclusion supported by theory (*3*). When two sets of nanoparticles are functionalized with linkers that contain different but complementary sticky ends, particles can only bind to particles of the opposite type. A bcc lattice is therefore the most stable for these binary systems (Fig. 1D), rather than an fcc lattice, as

[1]Department of Chemistry, Northwestern University, Evanston, IL 60208, USA. [2]International Institute for Nanotechnology, Northwestern University, Evanston, IL 60208, USA. [3]X-ray Science Division, Advanced Photon Source, Argonne National Laboratory, Argonne, IL 60439, USA. [4]Department of Materials Science and Engineering, Northwestern University, Evanston, IL 60208, USA.

*To whom correspondence should be addressed. E-mail: chadnano@northwestern.edu

Report Documentation Page

Form Approved
OMB No. 0704-0188

1. REPORT DATE	2. REPORT TYPE	3. DATES COVERED
14 OCT 2011		**00-00-2011 to 00-00-2011**

4. TITLE AND SUBTITLE	5a. CONTRACT NUMBER
Nanoparticle Superlattice Engineering with DNA	5b. GRANT NUMBER
	5c. PROGRAM ELEMENT NUMBER
6. AUTHOR(S)	5d. PROJECT NUMBER
	5e. TASK NUMBER
	5f. WORK UNIT NUMBER
7. PERFORMING ORGANIZATION NAME(S) AND ADDRESS(ES) **Northwestern University ,Department of Chemistry,2145 Sheridan Road,Evanston,IL,60208**	8. PERFORMING ORGANIZATION REPORT NUMBER
9. SPONSORING/MONITORING AGENCY NAME(S) AND ADDRESS(ES)	10. SPONSOR/MONITOR'S ACRONYM(S)
	11. SPONSOR/MONITOR'S REPORT NUMBER(S)

12. DISTRIBUTION/AVAILABILITY STATEMENT
Approved for public release; distribution unlimited

13. SUPPLEMENTARY NOTES

14. ABSTRACT

15. SUBJECT TERMS

16. SECURITY CLASSIFICATION OF:			17. LIMITATION OF ABSTRACT	18. NUMBER OF PAGES	19a. NAME OF RESPONSIBLE PERSON
a. REPORT **unclassified**	b. ABSTRACT **unclassified**	c. THIS PAGE **unclassified**	**Same as Report (SAR)**	**5**	

each NP in a bcc lattice possesses more nearest neighbors of the opposite particle type. Note that this rule holds for a wide range of nanoparticle diameters and oligonucleotide lengths, and it can therefore be used to make many fcc and bcc lattices with well-defined and predictable lattice parameters over the 25- to 150-nm range (figs. S2 and S3).

Rule 2: *When two lattices are of similar stability, the kinetic product can be produced by slowing the rate at which individual DNA linkers dehybridize and subsequently rehybridize.* For example, theoretical predictions show that, although they possess the same number of nearest neighbors, hcp lattices are slightly less stable than fcc lattices, and thus any hcp crystals observed would likely be kinetic products (*20*). Indeed, we have observed hcp lattices in these systems, but only as metastable structures that reorganize into fcc lattices upon annealing (*15*). Stable hcp lattices can be realized by annealing at lower solution temperatures and decreasing the local DNA density around a NP surface (Fig. 1E). These two changes both slow the DNA linker sticky end release and rehybridization rates necessary for crystallization, and promote lattice growth over lattice reorganization, thereby stabilizing initial kinetic products. For example, by using long DNA strands (~30 nm) and NPs bearing a small number of linkers (7.2-nm NPs, 20 ± 3 DNA strands per particle) and annealing at 25° to 30°C, one can preferentially stabilize the growth of initial hcp-like lattices that form during early time points of the assembly process (*15*). It is important to note that although this process can consistently be used to produce large (>1 μm) hcp lattices that are stable for extended periods of time (several weeks after formation), these structures are still kinetic products. Annealing hcp lattices at higher temperatures for several hours always results in the lattices reorganizing to an fcc structure (fig. S23).

Rule 3: *The overall hydrodynamic radius of a DNA-NP, rather than the sizes of its individual NP or oligonucleotide components, dictates its*

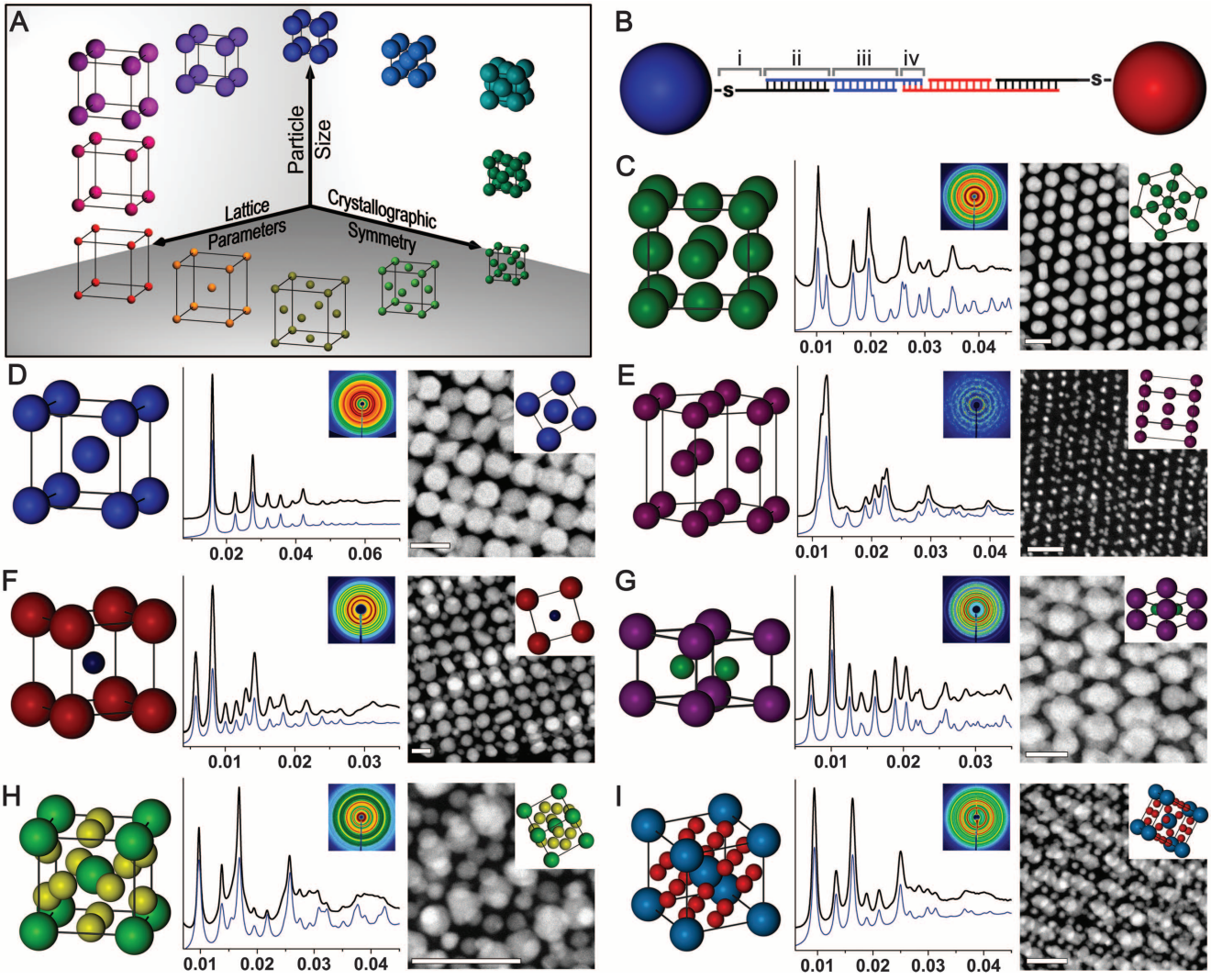

Fig. 1. (**A**) Nanoparticle superlattice engineering with DNA, unlike conventional particle crystallization, allows for independent control of three important design parameters (particle size, lattice parameters, and crystallographic symmetry) by separating the identity of the particle from the variables that control its assembly. (**B**) The DNA strands that assemble these nanoparticle superlattices consist of (i) an alkylthiol moiety and 10-base nonbinding region, (ii) a recognition sequence that binds to a DNA linker, (iii) a spacer sequence of programmable length to control interparticle distances, and (iv) a "sticky end" sequence that drives nanoparticle assembly via DNA hybridization interactions. Although only a single linkage is shown schematically here, DNA-NPs typically contain tens to hundreds of DNA linkers per particle. (**C** to **I**) The superlattices reported herein are isostructural with (C) fcc, (D) bcc, (E) hcp, (F) CsCl, (G) AlB_2, (H) Cr_3Si, and (I) Cs_6C_{60} lattices. From left to right, each panel contains a model unit cell (not to scale), 1D and 2D (inset) x-ray diffraction (SAXS) patterns, and a TEM image of resin-embedded superlattices, along with the unit cell viewed along the appropriate projection axis (inset). Lines in the model denote edges of the unit cell; individual DNA connections are omitted for clarity. SAXS data are plots of nanoparticle superlattice structure factor $S(q)$ (y axis, arbitrary units) versus scattering vector $\mathbf{q}$ (x axis, $Å^{-1}$). Black traces are experimental data; blue traces are modeled SAXS patterns for perfect lattices. All scale bars in the TEM images are 50 nm. See (*19*) for a complete list of particle sizes and lattice parameters.

assembly and packing behavior. An important aspect of DNA-NP design is that the overall hydrodynamic radius of a DNA-NP is a combination of the NP diameter and the DNA length. As each of these parameters is independently controllable, one can easily synthesize two DNA-NPs with the same overall hydrodynamic radius but different NP core sizes (Fig. 2A). Thus, we could assemble NPs into three-dimensional (3D) structures with lattice parameters and interparticle distances that are not dictated solely by the sizes of the inorganic particle cores.

This rule is well illustrated by the synthesis of CsCl lattices (Fig. 1F), which exhibit the same DNA-NP arrangement and connectivity as a bcc lattice but use two different NP core sizes. To create a range of CsCl lattices, we systematically changed the lengths of oligonucleotide linkers to obtain DNA-NPs with the appropriate hydrodynamic radii (Fig. 2B). Note that by simply changing the length of the oligonucleotide linkers, the inorganic particle radius and interparticle distance were independently programmed for nanoparticles ranging from 5 to 60 nm in diameter, with lattice parameters ranging from ~40 to ~140 nm. The inorganic NP core sizes in these lattices differed by as much as 30 nm and still exhibited equivalent packing and assembly behavior.

Rule 4: *In a binary system, the size ratio and DNA linker ratio between two particles dictate the thermodynamically favored crystal structure.* For this rule, the "size ratio" is defined as the ratio of the DNA-NPs' hydrodynamic radii (a sum of the inorganic particle radius and DNA linker length), and the DNA linker ratio is the ratio of the number of DNA linkers on the two different types of DNA-NPs. Size ratio can be predicted to affect the stability of different crystal symmetries because it determines the packing parameters of DNA-NPs within a lattice (i.e., the number and positions of adjacent particles to which a given DNA-NP can bind). The DNA linker ratio can also be expected to affect crystal stability, as it determines the number of DNA sticky ends available to form DNA connections with these adjacent particles. For example, by adjusting the size ratio of the DNA-NP components, lattices isostructural with AlB_2 can be obtained (Fig. 1G; size ratio 0.64). By varying both the size ratio and the DNA linker ratio, lattices isostructural with Cr_3Si can be made (Fig. 1H; size ratio 0.37, DNA linker ratio ~2)—an unusual example of a NP superlattice with this lower crystallographic symmetry. Finally, by using a DNA linker ratio of ~3, we synthesized a lattice that has no mineral equivalent but is isostructural with the alkali-fullerene complex Cs_6C_{60} (*21*) (Fig. 1I; size ratio ~0.35).

Note that the lattices in Fig. 1 are only individual examples of the many AlB_2, Cr_3Si, and Cs_6C_{60} crystals synthesized with this method. These structures also have been constructed using multiple particle sizes (5 to 30 nm) and hydrodynamic radii (10 to 50 nm) (figs. S6 to S8 and S17 to S19). By applying rule 3, one can tune the hydrodynamic radii of particles (and thus the hydrodynamic size ratio) to position particles into a specific crystallographic symmetry without being restricted to specific inorganic particle sizes or even to specific inorganic particle size ratios. Indeed, the hydrodynamic radii of the particles can even be tuned such that in a given system, the DNA-NP with the larger inorganic core size possesses the smaller hydrodynamic radius. In this way, one can position a given nanoparticle at any of the occupied Wyckoff positions within a given lattice type's unit cell, regardless of the inorganic particle's size (Fig. 2C).

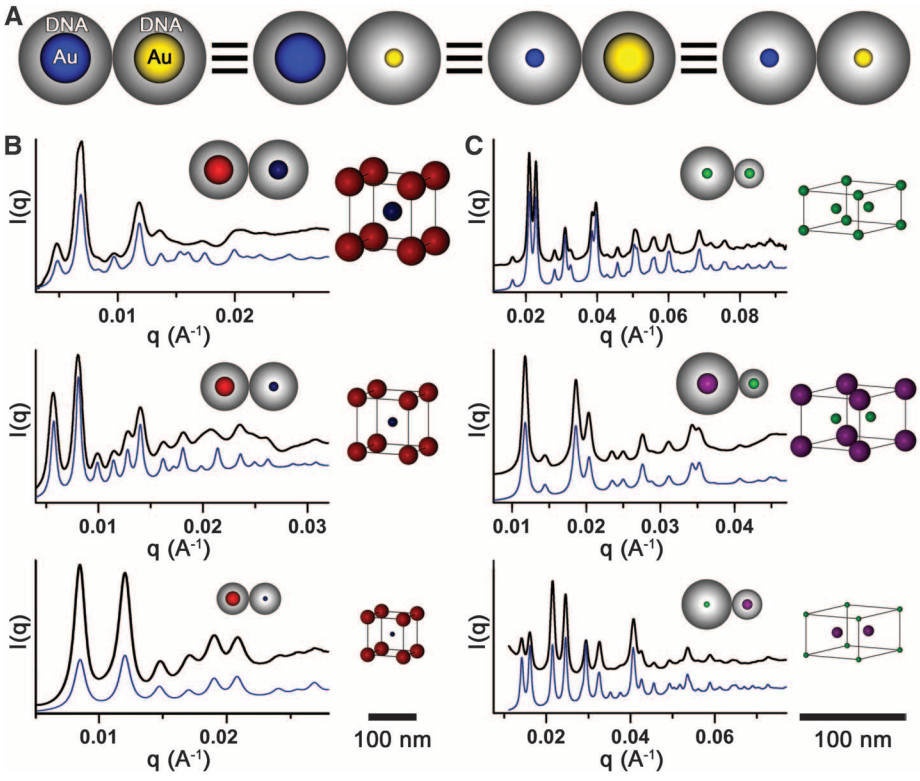

Fig. 2. (**A**) Two particles with the same hydrodynamic radius exhibit the same assembly behavior, regardless of the sizes of the inorganic nanoparticle cores. (**B**) SAXS patterns for CsCl lattices in binary systems where two particles have the same hydrodynamic radii but different inorganic core sizes. The inset and model show the relative sizes of the nanoparticles, DNA linkers, and assembled lattices, all drawn to scale. From top to bottom, the nanoparticle sizes are 60 and 40 nm, 40 and 20 nm, and 30 and 10 nm. (**C**) SAXS patterns for AlB_2 lattices, demonstrating that crystallographic symmetry and lattice parameters can be controlled independently of the sizes and size ratios of the inorganic nanoparticle cores (inset and model, both drawn to scale). From top to bottom, the inorganic core sizes of the "big" and "small" nanoparticles (as defined by their overall hydrodynamic radii) are 10 and 10 nm, 20 and 10 nm, and 5 and 10 nm. See (*19*) for exact interparticle distances and lattice parameters for all structures.

Rule 5: *Two systems with the same size ratio and DNA linker ratio exhibit the same thermodynamic product.* Note that crystal stability is determined by the ratio of the two variables discussed in rule 4, not their absolute values. A comparison of the lattices created with rule 4 shows that, regardless of the absolute values of DNA-NP size or the number of DNA linkers per particle, two systems with the same size ratios and DNA linker ratios form the same thermodynamic product. Consequently, the application of rule 5 as a guiding principle in superlattice assembly enables a large number of lattices to be synthesized without necessitating a complete reanalysis of the forces involved in assembly for each specific nanoparticle size or DNA length. Further, this result implies that one could construct a phase diagram that would predict the most stable crystal structure as a function of these two variables. As previously mentioned, the main hypothesis of this work states that the thermodynamic products in this assembly method are the ones that maximize DNA duplex formation. However, experimental verification of this hypothesis (and thus the development of a phase diagram) is challenging, as it is difficult to experimentally determine the number of DNA duplexes formed in a given lattice. Therefore, we have constructed a model that is based on the predictable and well-established properties of both DNA (persistence length, rise per base pair) (*22*) and DNA-NPs (number of DNA strands per particle, the hybridization behavior of sticky ends) (*16*) and used this model to calculate relative crystal stabilities.

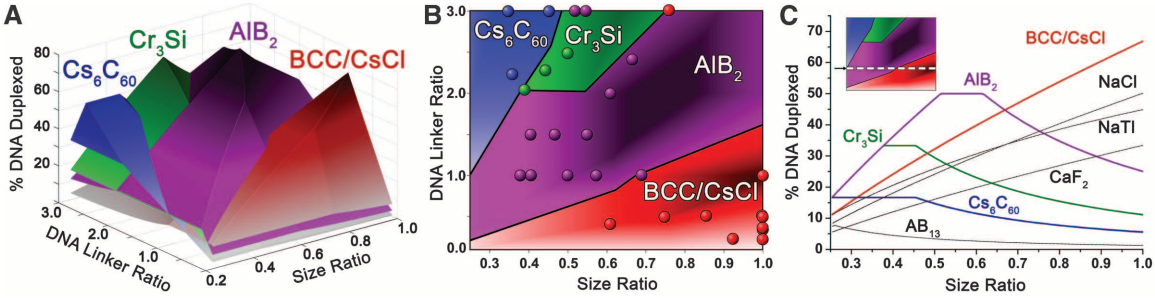

Fig. 3. (**A**) Surface plot of modeled data, in which the percentage of DNA sticky ends that form duplexes (*z* axis) is calculated for different crystallographic arrangements as a function of experimentally controllable design parameters (DNA linker ratio, *x* axis; DNA-NP size ratio, *y* axis). (**B**) Phase diagram constructed as a top-down view of (A), where each dot on the graph represents a lattice that was synthesized experimentally. The color of each experimental data point denotes the identity of the lattice obtained. (**C**) Two-dimensional "slice" through the plot in (B), at a constant DNA linker ratio of 1.0. This plot demonstrates the relative stability of both lattices that have been constructed with DNA-programmed assembly (color traces) and other lattices that have been theoretically predicted or synthesized using other assembly methodologies (black traces). The inset indicates where this slice was taken from (B).

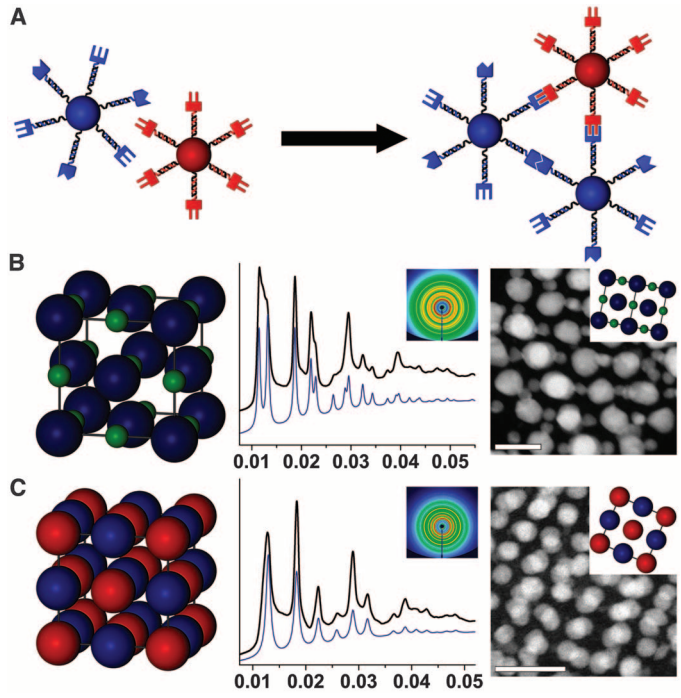

Fig. 4. (**A**) More complex nanoparticle assemblies can be created when programming multivalent DNA-NP interactions. For example, by encoding multiple distinct sticky end sequences on the same particle, both self-complementary and non–self-complementary interactions can be used to assemble lattices. (**B** and **C**) This strategy can be used to create a NaCl lattice (B) when using two particles with different inorganic core sizes, or a simple cubic lattice (C) when using two particles with the same inorganic core size. From left to right, each panel shows a model unit cell, 1D and 2D (inset) SAXS data, and a TEM image with the unit cell viewed along the appropriate projection axis (inset). In (B), the SAXS data correspond to a NaCl lattice with 15-nm and 10-nm AuNPs and the TEM image is of a NaCl lattice with 30-nm and 15-nm AuNPs. In (C), the SAXS data correspond to a simple cubic lattice with 10-nm AuNPs and the TEM image shows a simple cubic lattice with 15-nm AuNPs. Scale bars, 50 nm.

The foundations for this model (hereafter referred to as the complementary contact model, or CCM) are the assumptions that (i) DNA linker sticky ends must be able to physically contact one another to hybridize, and (ii) any sticky ends that can come into contact will eventually form a DNA duplex. The DNA linker strands on the surface of a DNA-NP are dynamic and can therefore be treated as a single collective entity (*16*). This allows one to represent a DNA-NP as a "fuzzy sphere" rather than a particle with a discrete set of DNA linkers. Because DNA linker sticky ends must physically contact one another to form a DNA duplex, it is therefore assumed that a greater amount of surface contact between adjacent spheres that contain complementary sticky ends correlates to a larger number of DNA duplexes being formed. By using the physical characteristics of the DNA-NP building blocks mentioned above, one can design a model lattice of arbitrary symmetry that has the appropriate lattice parameters (as dictated by a given set of particle sizes and DNA lengths), and then use the CCM to determine how many complementary sticky ends are able to contact one another and subsequently hybridize. This process enables the prediction of the number of DNA duplexes in a given crystal structure as a function of size ratio and DNA linker ratio (Fig. 3A) (*19*). If the main hypothesis of this work is correct, a larger number of DNA duplexes formed for a given crystal structure should correlate to a more stable lattice. Thus, the lattice with the most surface contact between adjacent complementary spheres should possess the greatest number of DNA duplexes and therefore should be the most stable phase for a given set of variables. Although the CCM is not intended to provide an explicit solution for determining the most stable crystal structure for a given set of design parameters, it should provide a suitable means to test both rule 5 and the hypothesis that maximization of DNA hybridization is the driving force for forming ordered crystals.

A comparison of the modeled phase diagram to experimentally obtained data shows that the model correctly predicts the structures obtained for a wide range of DNA-NP size ratios and DNA linker ratios, confirming the predominant hypothesis of this work as well as rules 4 and 5 (Fig. 3B). The model was also used to confirm that the lattices obtained experimentally are more stable than a number of other structures that have been predicted by previous theoretical calculations or that have been assembled with other methodologies (Fig. 3C) (*8*, *23*). Although there are limitations to the predictive nature of the CCM as it currently is constructed (*19*) (figs. S24 to S28), the vast majority of the data generated by the model are in complete agreement with the synthesized lattices. Given that all experimentally generated data points validate the six rules developed in this work, it is reasonable to assume that simplifications used to develop the CCM are the result of this discrepancy. Nonetheless, the strong agreement between experiment and theory demonstrates that the CCM should provide a solid basis for future computational work in this area. As a result, the control over experimental design parameters (hydrodynamic size ratios, inorganic particle radii, and DNA lengths) afforded by this DNA-based assembly method and coupled with the predictive nature of this phase diagram, allows one to determine the experimental variables necessary to create a diverse array of lattices a priori, with independent control over crystallographic symmetry, lattice parameters, and nanoparticle sizes (figs. S2 to S10 and S13 to S21).

Rule 6: *The most stable crystal structure will maximize all possible types of DNA sequence–specific hybridization interactions.* The examples

above examine relatively simple binary systems, where only a single type of DNA sticky end duplex is created. However, because of the polyvalent nature of the DNA-NPs and the base sequence programmability of DNA, one is not necessarily restricted to a single type of favorable particle interaction in a given lattice. By cofunctionalizing a nanoparticle with different linkers that contain different base sequences, multiple sequence-specific DNA duplex interactions are possible (Fig. 4A). This is an inherent distinction and potential advantage of using a sequence-programmable linker such as DNA, as opposed to entropy- or charge-dominated assembly processes.

This rule was tested by cofunctionalizing a nanoparticle with two different linkers: one that bore a self-complementary sticky end, and one that bore a sticky end sequence complementary to the sticky ends of a second particle. In this system, the cofunctionalized particle (blue particle, Fig. 4A) exhibited an attractive force with respect to all particles encountered in the system, whereas the second particle (red particle, Fig. 4A) was only attracted to the first particle type. When the hydrodynamic radius size ratio of the two NPs was ~0.3 to 0.4, the sticky ends were presented at the correct distances from the particle surface to form a NaCl lattice (Fig. 4B); that is, the self-complementary and non–self-complementary linkers were both at a position to form duplexes in this crystallographic arrangement. Furthermore, when the inorganic core sizes were the same on both DNA-NPs, the particles formed a simple cubic lattice, as defined by the positions of the inorganic cores (Fig. 4C). Although NaCl and simple cubic structures are presented as the first examples of this multivalent strategy, one can envision even more sophisticated and complex systems (such as lattices with three or more nanoparticle components) using multiple DNA-programmed NP interactions.

We have presented a set of basic design rules for synthesizing a diverse array of nanoparticle superlattices using DNA as a synthetically programmable linker. These rules provide access to an easily tailorable, multifaceted design space in which one can independently dictate the crystallographic symmetry, lattice parameters, and particle sizes within a lattice. This in turn enables the synthesis of many different nanoparticle superlattices that cannot be achieved through other methodologies. Indeed, superlattices that do not follow the well-known hard-sphere packing parameter rules defined by Schiffrin and co-workers (*6*) and Murray and co-workers (*8*, *24*) can easily be assembled as thermodynamically stable structures over a range of nanoparticle sizes and lattice parameters. The understanding gained from the use of these rules will both inform and enable future assembly efforts, allowing for the construction of new crystallographic arrangements that have emergent properties for use in the fields of plasmonics (*14*, *25*, *26*), photonics (*27*), catalysis (*28*, *29*), and potentially many others.

References and Notes

1. L. Pauling, *The Nature of the Chemical Bond* (Cornell Univ. Press, Ithaca, NY, ed. 3, 1960).
2. C. A. Mirkin, R. L. Letsinger, R. C. Mucic, J. J. Storhoff, *Nature* **382**, 607 (1996).
3. S.-J. Park, A. A. Lazarides, J. J. Storhoff, L. Pesce, C. A. Mirkin, *J. Phys. Chem. B* **108**, 12375 (2004).
4. S. Y. Park *et al*., *Nature* **451**, 553 (2008).
5. D. Nykypanchuk, M. M. Maye, D. van der Lelie, O. Gang, *Nature* **451**, 549 (2008).
6. C. J. Kiely, J. Fink, M. Brust, D. Bethell, D. J. Schiffrin, *Nature* **396**, 444 (1998).
7. A. M. Kalsin *et al*., *Science* **312**, 420 (2006); 10.1126/science.1125124.
8. E. V. Shevchenko, D. V. Talapin, N. A. Kotov, S. O'Brien, C. B. Murray, *Nature* **439**, 55 (2006).
9. S. Srivastava *et al*., *Science* **327**, 1355 (2010); 10.1126/science.1177218.
10. S. Wong, V. Kitaev, G. A. Ozin, *J. Am. Chem. Soc.* **125**, 15589 (2003).
11. Y. Zhao *et al*., *Nat. Mater.* **8**, 979 (2009).
12. C.-L. Chen, N. L. Rosi, *Angew. Chem. Int. Ed.* **49**, 1924 (2010).
13. Z. Nie, A. Petukhova, E. Kumacheva, *Nat. Nanotechnol.* **5**, 15 (2010).
14. M. R. Jones, K. D. Osberg, R. J. Macfarlane, M. R. Langille, C. A. Mirkin, *Chem. Rev.* **111**, 3736 (2011).
15. R. J. Macfarlane *et al*., *Proc. Natl. Acad. Sci. U.S.A.* **106**, 10493 (2009).
16. R. J. Macfarlane *et al*., *Agnew. Chem. Int. Ed.* **49**, 4589 (2010).
17. M. R. Jones *et al*., *Nat. Mat.* **9**, 913 (2010).
18. H. Xiong, D. van der Lelie, O. Gang, *Phys. Rev. Lett.* **102**, 015504 (2009).
19. See supporting material on *Science* online.
20. L. V. Woodcock *et al*., *Nature* **385**, 141 (1997).
21. O. Zhou *et al*., *Nature* **351**, 462 (1991).
22. V. A. Bloomfield, D. M. Crothers, I. Tinoco, *Nucleic Acids: Structures, Properties, and Functions* (University Science Books, Sausalito, CA, 2000).
23. A. V. Tkachenko, *Phys. Rev. Lett.* **89**, 148303 (2002).
24. M. I. Bodnarchuk, M. V. Kovalenko, W. Heiss, D. V. Talapin, *J. Am. Chem. Soc.* **132**, 11967 (2011).
25. K. L. Kelly, E. Coronado, L. L. Zhao, G. C. Schatz, *J. Phys. Chem. B* **107**, 668 (2002).
26. J. A. Fan *et al*., *Science* **328**, 1135 (2010).
27. K. J. Stebe, E. Lewandowski, M. Ghosh, *Science* **325**, 159 (2009).
28. A. T. Bell, *Science* **299**, 1688 (2003).
29. J. Grunes, J. Zhu, E. A. Anderson, G. A. Somorjai, *J. Phys. Chem. B* **106**, 11463 (2002).

Acknowledgments: Supported by the Defense Research & Engineering Multidisciplinary University Research Initiative of the Air Force Office of Scientific Research and by the U.S. Department of Energy Office of Basic Energy Sciences [award DE-SC0000989; Northwestern University (NU) Non-equilibrium Energy Research Center] (C.A.M. and G.C.S.); a National Security Science and Engineering Faculty Fellowship from the U.S. Department of Defense (C.A.M.); a NU Ryan Fellowship (R.J.M.); and a NU Ryan Fellowship and a NSF Graduate Research Fellowship (M.R.J.). Portions of this work were carried out at the DuPont-Northwestern-Dow Collaborative Access Team (DND-CAT) beamline located at Sector 5 of the Advanced Photon Source (APS). DND-CAT is supported by E. I. DuPont de Nemours & Co., Dow Chemical Company, and the state of Illinois. Use of the APS was supported by the U.S. Department of Energy, Office of Science, Office of Basic Energy Sciences, under contract DE-AC02-06CH11357. The transmission electron microscope work was carried out in the EPIC facility of the NU Atomic and Nanoscale Characterization Experimental Center, which is supported by NSF-NSEC, NSF-MRSEC, Keck Foundation, the state of Illinois, and NU. Ultrathin sectioning was carried out at the NU Biological Imaging Facility, supported by the NU Office for Research.

Supporting Online Material

www.sciencemag.org/cgi/content/full/334/6053/204/DC1
Materials and Methods
SOM Text
Figs. S1 to S31
Tables S1 and S2
References (*30*–*44*)

29 June 2011; accepted 25 August 2011
10.1126/science.1210493

Conical Intersection Dynamics in NO_2 Probed by Homodyne High-Harmonic Spectroscopy

H. J. Wörner,[1,2]* J. B. Bertrand,[1] B. Fabre,[3] J. Higuet,[3] H. Ruf,[3] A. Dubrouil,[3] S. Patchkovskii,[1] M. Spanner,[1] Y. Mairesse,[3] V. Blanchet,[4] E. Mével,[3] E. Constant,[3] P. B. Corkum,[1] D. M. Villeneuve[1]

Conical intersections play a crucial role in the chemistry of most polyatomic molecules, ranging from the simplest bimolecular reactions to the photostability of DNA. The real-time study of the associated electronic dynamics poses a major challenge to the latest techniques of ultrafast measurement. We show that high-harmonic spectroscopy reveals oscillations in the electronic character that occur in nitrogen dioxide when a photoexcited wave packet crosses a conical intersection. At longer delays, we observe the onset of statistical dissociation dynamics. The present results demonstrate that high-harmonic spectroscopy could become a powerful tool to highlight electronic dynamics occurring along nonadiabatic chemical reaction pathways.

The outcome of chemical reactions is determined by the valence electronic structure of molecules. Therefore, the elucidation of elementary reaction mechanisms requires an understanding of the valence electron dynamics. Recently developed techniques that are efficient in probing valence electron dynamics include attosecond transient absorption (*1*), extreme ultraviolet photoelectron spectroscopy (XUV-PES) (*2*), high-order harmonic spectroscopy (HHS) (*3*–*5*) and strong-field ionization (*6*). Both time-resolved PES (*7*) and time-resolved HHS are